JACS
JOURNAL OF THE AMERICAN CHEMICAL SOCIETY
Communication
pubs.acs.org/JACS

Evidence for Anionic Excess Electrons in a Quasi-Two-Dimensional Ca_2N Electride by Angle-Resolved Photoemission Spectroscopy

Ji Seop Oh,[†,§] Chang-Jong Kang,[‡] Ye Ji Kim,[∥,⊥] Soobin Sinn,[†,§] Moonsup Han,[#] Young Jun Chang,[#] Byeong-Gyu Park,[¶] Sung Wng Kim,[∥] Byung Il Min,[‡] Hyeong-Do Kim,[*,†,§] and Tae Won Noh[†,§]

[†]Center for Correlated Electron Systems, Institute for Basic Science, Seoul 151-742, Korea
[§]Department of Physics & Astronomy, Seoul National University, Seoul 151-742, Korea
[‡]Department of Physics, Pohang University of Science and Technology, Pohang 790-784, Korea
[∥]Department of Energy Science, Sungkyunkwan University, Suwon 440-746, Korea
[⊥]Center for Integrated Nanostructure Physics, Institute for Basic Science, Suwon 440-746, Korea
[#]Department of Physics, University of Seoul, Seoul 130-743, Korea
[¶]Pohang Accelerator Laboratory, Pohang University of Science and Technology, Pohang 790-784, Korea

ABSTRACT: Angle-resolved photoemission spectroscopy (ARPES) study of a layered electride Ca_2N was carried out to reveal its quasi-two-dimensional electronic structure. The band dispersions and the Fermi-surface map are consistent with the density functional theory results except for a chemical potential shift that may originate from the high reactivity of surface excess electrons. Thus, the existence of anionic excess electrons in the interlayer region of Ca_2N is strongly supported by ARPES.

Electrides are exotic materials, in which electrons play a role as anions. They have attracted a great deal of attention because of their intriguing chemical properties.[1−3] Despite the presence of seemingly highly reactive excess electrons, a thermally and chemically stable $[Ca_{24}Al_{28}O_{64}]^{4+}(4e^-)$ electride[4] was synthesized and has been utilized in various areas such as field emission[5] and ammonia synthesis.[6] Inherent excess anionic electrons in most electrides are captured in zero-dimensional confining potential and can be localized[7] or delocalized in a network of confining sites,[8−10] showing various types of electrical conduction from variable range hopping to superconductivity.[11]

More than a decade ago, a subnitride Ca_2N with a layer structure[12] was proposed to have metallic two-dimensional (2D) excess electrons in the "van der Waals" gap between the calcium layers both by density functional theory (DFT) calculations[13] and by transport measurements on microcrystalline samples.[14] Recently, Lee et al. succeeded in synthesizing large single crystals of Ca_2N and in reporting highly anisotropic transport properties, confirming that Ca_2N is a metallic 2D electride in terms of $[Ca_2N]^+e^-$,[15,16] thus attracting much attention. Figure 1a shows the crystal structure of Ca_2N. The interlayer distance between Ca^{2+} ions (3.86 Å) is larger than the Ca−N bond length (2.44 Å).[12,13] Since Ca^{2+} ions are located at the outermost positions of each slab, the interlayer region could become electrostatically stable for electrons.[17] They used DFT calculations to show that excess electrons (indicated by the blue color in Figure 1a) from the slab reside in a 2D interlayer region between Ca^{2+} layers.[15,16] If realized, the interstitial

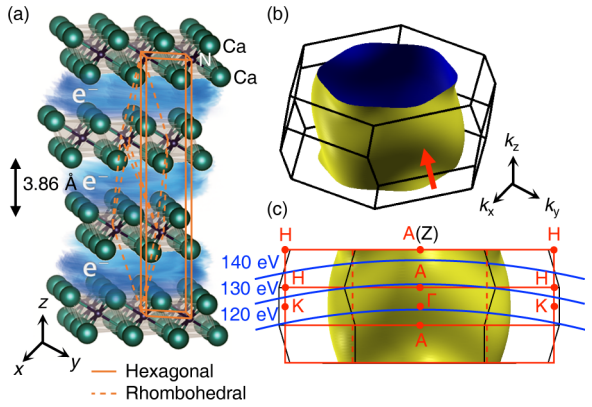

Figure 1. (a) Crystal structure, (b) the FS and the first BZ of Ca_2N in a 3D plot, and (c) the projected FS in which both hexagonal (red lines) and rhombohedral (black lines) unit cells are shown. Presumed probing paths of ARPES in the BZ at $h\nu$ = 120, 130, and 140 eV are depicted by blue lines.

electrons will occupy the topmost part of the valence bands, because their binding energies will be weaker than those of other valence electrons due to their nearly free binding nature. Then, most physical properties would become dominated by interstitial electrons with quasi-2D characteristics, which would be useful for electronic device applications. Motivated by this work, several candidates for 2D electrides have been intensively searched for based on the DFT.[17−20]

Despite extensive studies on electrides, convincing evidence for the existence of electrons as anions is rare. A most direct experimental method will be a charge-density mapping by X-ray diffraction (XRD) using the maximum entropy method combined with the Rietveld analysis. This method was carried out for another electride $12CaO{\cdot}7Al_2O_3$.[21] Unfortunately, such measurements are unlikely at present because the density of interstitial electrons is too low to be probed by XRD.[2] Plausible experimental evidence has been obtained only in comparative studies with their alkalide counterparts.[22−24] DFT calculations

Received: December 4, 2015
Published: February 3, 2016

DOI: 10.1021/jacs.5b12668
J. Am. Chem. Soc. 2016, 138, 2496−2499

have been widely employed to calculate the electronic structure of electrides. From the electronic structures and associated electron density maps, theoretical studies showed that excess electrons populate interstitial regions.[25] However, there has been no direct experimental confirmation of the DFT predictions. Therefore, it is necessary to perform electron spectroscopy studies in an ultrahigh vacuum and at a cryogenic temperature to reduce the reactivity of the electrides. Among them, angle-resolved photoemission spectroscopy (ARPES) is particularly useful in that it can directly measure electronic band dispersions with high energy and momentum resolutions.[26] Thus, compared with the DFT results, ARPES spectra can provide convincing experimental evidence for the existence of anionic electrons.

Here, we studied the electronic structure of Ca_2N using ARPES. A Fermi surface (FS) map and electronic energy-momentum dispersions at several photon energies were obtained and found to be consistent with DFT calculations. Hence, the quasi-2D nature of its electronic structure is successfully revealed by experimental approaches, and the existence of anionic electrons in the interlayer region of Ca_2N is strongly supported.

We grew single-crystalline Ca_2N samples as described previously.[15,16] To prevent unintended contamination during sample preparation, we used a glovebox filled up with a 99.999% Ar gas. We glued the single crystals on ARPES sample holders and aligned the sample azimuthal orientation within 2° by looking at the shape of the crystals. Then, we attached alumina posts to their top surfaces for the sample cleavage process. We also applied ultrahigh-vacuum grease (Apiezon N grease, Apiezon) to the remaining sample surface to prevent potential degradation. Then, we inserted the samples as quickly as possible into a load-lock chamber connected to an ARPES measurement chamber. After obtaining a fresh surface by *in situ* cleaving, we performed ARPES measurements at the 4A1 Beamline of PLS-II with a Scienta R4000 analyzer. We kept the base pressure of an analyzer chamber below 2×10^{-11} Torr and the sample temperature at 100 K. We could obtain ARPES spectra at several limited photon energies of 120, 130, and 140 eV because of too fast sample degradation. Total energy resolution was about 50 meV. We performed DFT calculations by using the full-potential linearized augmented plane-wave method, as implemented in the WIEN2K package.[27] For the exchange−correlation, we utilized the generalized gradient approximation of Perdew, Burke, and Ernzerhof.[28]

FS topology is the key to determine the dimensionality of a metal. As shown in Figure 1a, Ca_2N has a rhombohedral structure, but a hexagonal unit cell is used by convention. Figure 1b shows the three-dimensional (3D) display of the FS of Ca_2N from DFT calculations in the first Brillouin zone (BZ). The black boundary is from the rhombohedral primitive cell. As this 3D figure is complex and difficult to understand, we replotted the FS in Figure 1c by projecting along the red arrow in Figure 1b. The red lines show the slab-shaped BZ in the hexagonal conventional cell, the zone-boundary length along the *c*-axis of which is one-third that of the rhombohedral cell. The yellow object shows the FS, the shape of which is a warped open cylinder along the *c*-axis. Note that Ca_2N possesses a quasi-2D electronic structure at least in its FS as inferred in the layered crystal structure.

In ARPES, photons with different energies will probe different paths in the *k*-space, especially along the k_z direction. Therefore, it is highly desirable to measure ARPES with many incident photon energies to cover the whole BZ. However, Ca_2N single crystals are highly vulnerable to environmental conditions, so the *in situ* cleaved surface became degraded rapidly even at 2×10^{-11} Torr. Due to these experimental constraints, we obtained ARPES spectra at $h\nu$ = 120, 130, and 140 eV. Figure 1c shows presumed probing paths assuming an inner potential V_0 = 16.6 eV, the sum of the minimum value of the N 2s (12.3 eV) band and the work function of the electron analyzer (4.3 eV).

To examine the band dispersions of Ca_2N, we measured ARPES spectra at $h\nu$ = 140 and 130 eV in the Γ*KHA* plane. Figure 2a,b shows the results after normalizing by the maximum

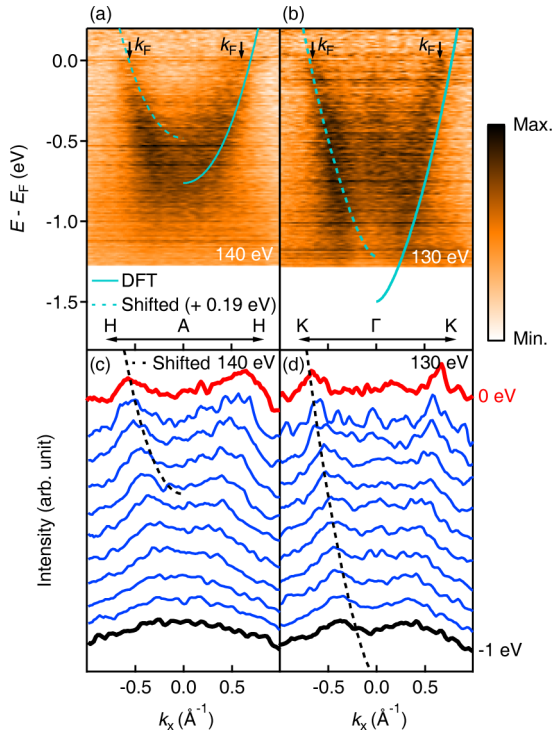

Figure 2. ARPES spectra of Ca_2N at $h\nu$ = (a) 140 and (b) 130 eV and (c, d) momentum distribution curves corresponding to (a, b), respectively. Solid and dashed lines are from DFT calculations.

and minimum values along each row and column. Both spectra show similar values of Fermi momenta denoted by k_F in the figures. However, the values of the band minima are quite different from each other. At $h\nu$ = 140 eV, the value is about −0.7 eV, while that at $h\nu$ = 130 eV is lower than −1.3 eV. Thus, there should be considerable band dispersion along the *c*-axis as predicted by the DFT calculations.[13,15,16]

Let us first compare the band dispersion from the ARPES data at $h\nu$ = 140 eV and the DFT calculations. Since the value of the band minimum is similar to that at the high-symmetry $A(Z)$ point (the *A* point corresponds to the *Z* point in the rhombohedral unit cell), we compare along the *A*−*H* line, as shown by the green solid line in Figures 2a. As clearly seen in the figure, the value of k_F is a little smaller in ARPES. This discrepancy is likely due to the depletion of excess electrons on the cleaved surface. Since these electrons are not confined between two Ca^{2+} layers as in the bulk and are exposed to residual gases such as H_2O and CO in the vacuum chamber, they will promptly form insulating contaminants on the surface. Thus, the chemical potential on the surface moves downward

DOI: 10.1021/jacs.5b12668
J. Am. Chem. Soc. 2016, 138, 2496−2499

and k_F decreases. A significant charge transfer from excess electrons in a Ca_2N monolayer to adsorbates was also reported based on DFT calculations.[29] To match the k_F values, we shifted the DFT band dispersion upward by 0.19 eV, shown as a dashed green line on the left side of Figure 2a. Overall agreement is quite good, and a mismatch may originate from the difference in probing path shown in Figure 1c or from the maltreatment of the exchange−correlation function in the DFT calculations.

A similar comparison was also made for ARPES spectra at $h\nu$ = 130 eV in Figure 2b. Here, the DFT dispersion along the Γ−*K* line was employed because the *c*-axis dispersion is negligible up to the midpoint of the Γ−$A(Z)$ line.[13,15,16] The much faster dispersion than at $h\nu$ = 130 eV is well matched between the ARPES spectra and the DFT calculations. For clearer comparison, Figure 2c,d shows momentum distribution curves (MDCs) consecutively from −1.0 to 0.0 eV by summing over an energy window of 50 meV to enhance the signal-to-noise ratio. Dispersions from the DFT shifted by 0.19 eV are overlapped by dashed lines. The calculated dispersions show a good agreement with the peaks from MDCs.

Figure 3 shows the FS map obtained from ARPES spectra at $h\nu$ = 120 eV, integrated by an energy window of 50 meV

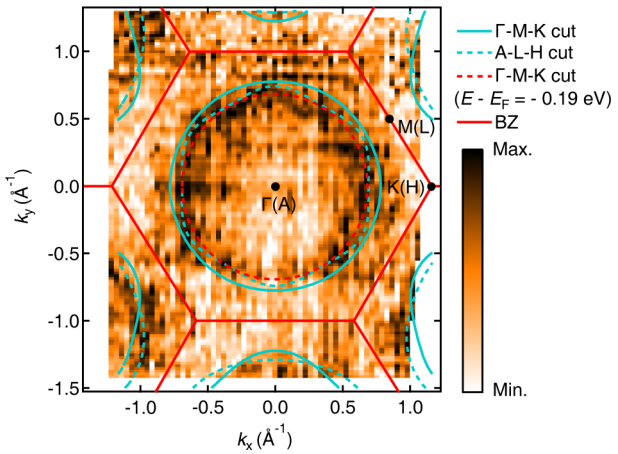

Figure 3. FS map obtained from ARPES spectra at $h\nu$ = 120 eV. FS cuts (green solid and dashed lines) and a constant-energy surface at −0.19 eV in the Γ*KHA* plane (red dashed line) are also shown for comparison.

centered at the Fermi level. The map was normalized by the same method as used in Figure 2. Although the ARPES data are not of high quality due to rapid sample degradation, we can still discern the FS with a near-circular shape. We also plotted FS boundaries by green solid and dashed lines from the DFT calculations projected along the *c*-axis. Both results show a good agreement in shape, but the size is a little smaller in the experimental one, possibly due to the depletion of excess electrons on the cleaved surface as explained previously. Better agreement is found in comparison with a constant-energy surface at −0.19 eV in the Γ*KHA* plane (red dashed line) to mimic the chemical potential shift in the ARPES data. Although we could not measure the whole region in the Γ−$A(Z)$ line, the FS is quasi-2D because the values of k_F measured at $h\nu$ = 120, 130, and 140 eV show little difference.

Taking the slight chemical potential shift into account, there are reasonably good agreements between ARPES and DFT results in the FS map and the band dispersions. These agreements suggest that all other DFT results can reliably describe the electronic structure of Ca_2N. For example, the electron density map obtained by the DFT in ref 15 suggests that excess electrons reside in the interlayer regions. If not, there should be hybridizations between electrons different from the DFT predictions, thus markedly changing the whole band topology. Note that the predicted excess-electron density in the interlayer regions[15,16] is too low to be detected directly by XRD. In this sense, ARPES can provide plausible evidence regarding the existence of interstitial electrons when combined with DFT calculations. Additionally, the good agreement between the ARPES spectra and the DFT results implies that electron−electron correlations are negligible in the electronic structure of Ca_2N.

A remaining puzzle of our ARPES spectra is that the band dispersion along the *c*-axis is as fast as that along the in-plane direction. Similar behavior was also shown in the DFT results (Figure 3a of ref 15). When excess electrons play a role as anions in the interlayer region, they bridge Ca_2N layers to facilitate movement along the *c*-axis. Then, the electronic structure should be 3D in contrast to our observation of quasi-2D FS, which was also questioned in ref 29.

This puzzle may be resolved by investigating the orbital characters of the band that forms the FS. Figure 4 shows the

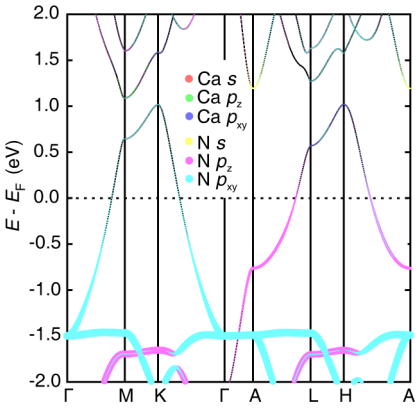

Figure 4. Orbital characters of the FS-forming band in Ca_2N.

orbital characters of the FS-forming band at the Ca and N sites. This figure does not show the orbital characters of excess electrons in interstitial regions. Since their bases are plane waves, they cannot be projected onto atomic orbital characters. In the Γ*MK* plane, i.e., k_z = 0, the in-plane N $2p_{x,y}$ orbitals are dominant. In contrast, the N $2p_z$ orbital contributions are considerable in the *ALH* plane. Then, we can understand the electronic structure of Ca_2N as follows. In the Γ*MK* plane, the band dispersion should be larger than in the *ALH* plane due to dominant in-plane orbital characters. As the momentum increases along the *c*-axis, the band rapidly approaches but still lies well below the Fermi level because of the short length of the Γ−$A(Z)$ line. In the *ALH* plane, the dispersion is markedly reduced because of strong out-of-plane orbital characters. As a result, the value of k_F is not much different from that in the Γ*MK* plane and the FS is quasi-2D.

In summary, we studied the electronic structure of an electride Ca_2N using ARPES. By varying photon energies, we can see considerable dispersion in ARPES spectra along the *c*-axis, but the values of k_F are not much different. Thus, confirming the quasi-2D nature of the electronic structure of

DOI: 10.1021/jacs.5b12668
J. Am. Chem. Soc. 2016, 138, 2496−2499

Ca_2N. Good agreement between ARPES and DFT results guarantees that all of the DFT results are reliable, thus providing firm evidence for the existence of anionic excess electrons in the interlayer region of Ca_2N.

AUTHOR INFORMATION

Corresponding Author

*hdkim6612@snu.ac.kr

Notes

The authors declare no competing financial interest.

ACKNOWLEDGMENTS

This work was supported by the Research Center Program of IBS (Institute for Basic Science) in Korea (IBS-R009-D1), the KISTI supercomputing center (no. KSC-2015-C3-007), and by the National Research Foundation of Korea (NRF) grant funded by the Korea government (MOE) (NRF-2012R1A1A2043619) and (MSIP) (NRF-2013R1A1A1008025, NRF-2014R1A1A1002868). M.H. was supported by the Sabbatical Program of University of Seoul.

REFERENCES

(1) Dye, J. L. *Science* **1990**, *247*, 663.
(2) Dye, J. L. *Inorg. Chem.* **1997**, *36*, 3816.
(3) Dye, J. L. *Acc. Chem. Res.* **2009**, *42*, 1564.
(4) Matsuishi, S.; Toda, Y.; Miyakawa, M.; Hayashi, K.; Kamiya, T.; Hirano, M.; Tanaka, I.; Hosono, H. *Science* **2003**, *301*, 626.
(5) Toda, Y.; Matsuishi, S.; Hayashi, K.; Ueda, K.; Kamiya, K.; Hirano, M.; Hosono, M. *Adv. Mater.* **2004**, *16*, 685.
(6) Kitano, M.; Inoue, Y.; Yamazaki, Y.; Hayashi, F.; Kanbara, S.; Matsuishi, S.; Yokoyama, T.; Kim, S.-W.; Hara, M.; Hosono, H. *Nat. Chem.* **2012**, *4*, 934.
(7) Sushko, P. V.; Shluger, A. L.; Hayashi, K.; Hirano, M.; Hosono, H. *Phys. Rev. Lett.* **2003**, *91*, 126401.
(8) Medvedeva, J. E.; Freeman, A. *Appl. Phys. Lett.* **2004**, *85*, 955.
(9) Sushko, P. V.; Shluger, A. L.; Hirano, M.; Hosono, H. *J. Am. Chem. Soc.* **2007**, *129*, 942.
(10) Kim, S. W.; Matsuishi, S.; Nomura, T.; Kubota, Y.; Takata, M.; Hayashi, K.; Kamiya, T.; Hirano, M.; Hosono, H. *Nano Lett.* **2007**, *7*, 1138.
(11) Miyakawa, M.; Kim, S. W.; Hirano, M.; Kohama, Y.; Kawaji, H.; Atake, T.; Ikegami, H.; Kono, K.; Hosono, H. *J. Am. Chem. Soc.* **2007**, *129*, 7270.
(12) Keve, E. T.; Skapski, A. C. *Chem. Commun.* **1966**, *22*, 829.
(13) Fang, C. M.; de Wijs, G. A.; de Groot, R. A.; Hintzen, H. T.; de With, G. *Chem. Mater.* **2000**, *12*, 1847.
(14) Gregory, D. H.; Bowman, A.; Baker, C. F.; Weston, D. P. *J. Mater. Chem.* **2000**, *10*, 1635.
(15) Lee, K.; Kim, S. W.; Toda, Y.; Matsuishi, S.; Hosono, H. *Nature* **2013**, *494*, 336.
(16) Inoshita, T.; Jeong, S.; Hamada, N.; Hosono, H. *Phys. Rev. X* **2014**, *4*, 031023.
(17) Tada, T.; Takemoto, S.; Matsuishi, S.; Hosono, H. *Inorg. Chem.* **2014**, *53*, 10347.
(18) Zhang, X.; Xiao, Z.; Hechang, L.; Toda, Y.; Matsuishi, S.; Kamiya, T.; Ueda, S.; Hosono, H. *Chem. Mater.* **2014**, *26*, 6638.
(19) Guan, S.; Yang, S. A.; Zhu, L.; Hu, J.; Yao, Y. *Sci. Rep.* **2015**, *5*, 12285.
(20) Nomura, T.; Hayashi, K.; Kubota, Y.; Kamiya, T.; Hirano, M.; Takata, M.; Hosono, H. *Chem. Lett.* **2007**, *36*, 902.
(21) Ellaboudy, A. S.; Bender, C. J.; Kim, J.; Shin, D. H.; Kuohenmeister, M. E.; Baboook, G. T.; Dye, J. L. *J. Am. Chem. Soc.* **1991**, *113*, 2347.
(22) McCracken, J.; Shin, D. H.; Dye, J. L. *Appl. Magn. Reson.* **1992**, *3*, 305.
(23) Kuchenmeister, M. E.; Dye, J. L. *J. Am. Chem. Soc.* **1989**, *111*, 935.
(24) Dale, S. G.; Otero-de-la-Roza, A.; Johnson, E. R. *Phys. Chem. Chem. Phys.* **2014**, *16*, 14584.
(25) Damascelli, A.; Hussain, Z.; Shen, Z.-X. *Rev. Mod. Phys.* **2003**, *75*, 473.
(26) Blaha, P.; Schwarz, K.; Madsen, G.; Kvasnicka, D.; Luitz, J. *WIEN2k*; Vienna University of Technology; Vienna, Austria, 2001.
(27) Perdew, J. P.; Burke, K.; Ernzerhof, M. *Phys. Rev. Lett.* **1997**, *78*, 1396.
(28) Zhao, S.; Li, Z.; Yang, J. *J. Am. Chem. Soc.* **2014**, *136*, 13313.
(29) Walsh, A.; Scanlon, D. O. *J. Mater. Chem. C* **2013**, *1*, 3525.

DOI: 10.1021/jacs.5b12668
J. Am. Chem. Soc. 2016, 138, 2496−2499